Stem Cell Reports
Article
OPEN ACCESS

3D Reconstitution of the Patterned Neural Tube from Embryonic Stem Cells

Andrea Meinhardt,[1] Dominic Eberle,[1] Akira Tazaki,[1] Adrian Ranga,[4] Marco Niesche,[2] Michaela Wilsch-Bräuninger,[3] Agnieszka Stec,[1] Gabriele Schackert,[2] Matthias Lutolf,[4] and Elly M. Tanaka[1,3,*]
[1]DFG-Research Center for Regenerative Therapies, Technische Universität Dresden, 01307 Dresden, Germany
[2]Neurosurgery Department, Faculty of Medicine, Technische Universität Dresden, 01307 Dresden, Germany
[3]Max Planck Institute of Molecular Cell Biology and Genetics, 01307 Dresden, Germany
[4]Laboratory of Stem Cell Bioengineering, Institute of Bioengineering, Ecole Polytechnique Fédérale de Lausanne, 1015 Lausanne, Switzerland
*Correspondence: elly.tanaka@crt-dresden.de
http://dx.doi.org/10.1016/j.stemcr.2014.09.020

SUMMARY

Inducing organogenesis in 3D culture is an important aspect of stem cell research. Anterior neural structures have been produced from large embryonic stem cell (ESC) aggregates, but the steps involved in patterning such complex structures have been ill defined, as embryoid bodies typically contained many cell types. Here we show that single mouse ESCs directly embedded in Matrigel or defined synthetic matrices under neural induction conditions can clonally form neuroepithelial cysts containing a single lumen in 3D. Untreated cysts were uniformly dorsal and could be ventralized to floor plate (FP). Retinoic acid posteriorized cysts to cervical levels and induced localize FP formation yielding full patterning along the dorsal/ventral (DV) axis. Correct spatial organization of motor neurons, interneurons, and dorsal interneurons along the DV axis was observed. This system serves as a valuable tool for studying morphogen action in 3D and as a source of patterned spinal cord tissue.

INTRODUCTION

Recently, substantial progress has been made to elicit organogenesis in 3D culture (Antonica et al., 2012; Huch et al., 2013; Liu et al., 2010; Sato et al., 2009; Spence et al., 2011). In the neural lineage, embryoid body-like aggregates were used to generate structures of the cerebral cortex, the pituitary gland, and the retina, three anterior regions of the neuraxis (Eiraku et al., 2008, 2011; Nakano et al., 2012; Suga et al., 2011). In the reconstituted cortex or retina, embryonic stem cell (ESC) differentiation led to the self-formation of layered structures containing different types of neurons. So far, self-organization in CNS organoids has been achieved using large, preaggregated cultures consisting of 3,000 to 10,000 cells, a condition where local inhomogeneities arise to promote complex tissue formation. The contribution of nonneural cells secreting signaling molecules could also not be excluded. Spinal cord level cells have already been induced from mouse embryonic stem cells (mESCs) in the context of complex embryoid bodies that contained a mixture of cells from different germ layers (Okada et al., 2008; Wichterle et al., 2002).

Here, we induce neural tube formation from mESCs by direct embedding of single-cell suspensions under neural induction conditions. Untreated, these 3D neuroepithelia have dorsal identity but respond to the ventralizing influence of sonic hedgehog (SHH). Upon retinoic acid (RA) addition, they are posteriorized to cervical levels but also spontaneously form a localized floor plate (FP). This FP elicits full dorsal/ventral (DV) patterning, including motor neurons (MNs) and ventral and dorsal interneurons. Such a system will have numerous uses for studying the mechanism of morphogen action in a 3D environment, as well providing a source of patterned spinal cord tissue.

RESULTS

3D Differentiation of mESCs into Polarized Neuroepithelial Cysts

We sought to generate a 3D culture system for neural progenitors that reproduces the growth and patterning of the embryonic spinal cord. Single cell suspensions of mouse ESCs from three ESC lines (R1, the SOX1::GFP reporter cell line 46C [Aubert et al., 2003] and IB10) were embedded in a 3D Matrigel matrix and differentiated along the neural lineage in N2B27 medium (Figure 1A). With all three cell lines in the presence or absence of Noggin, we obtained spherical- to ellipsoid-shaped structures that possessed a single lumen (Figure 1B) and reached similar though not identical sizes (Figure S1A available online). The presence of a single lumen makes these structures similar to epithelial cysts as previously described for kidney epithelial cells (O'Brien et al., 2001; Yu et al., 2005) and distinguishes them from embryoid bodies or floating aggregates (Eiraku et al., 2008; Elkabetz et al., 2008; Lazzari et al., 2006), so we refer to our structures as neuroepithelial cysts.

Confocal analysis of immunostained cysts revealed the hallmarks of early neuroepithelial tissue, including apical-basal polarity reflected by apical localization of

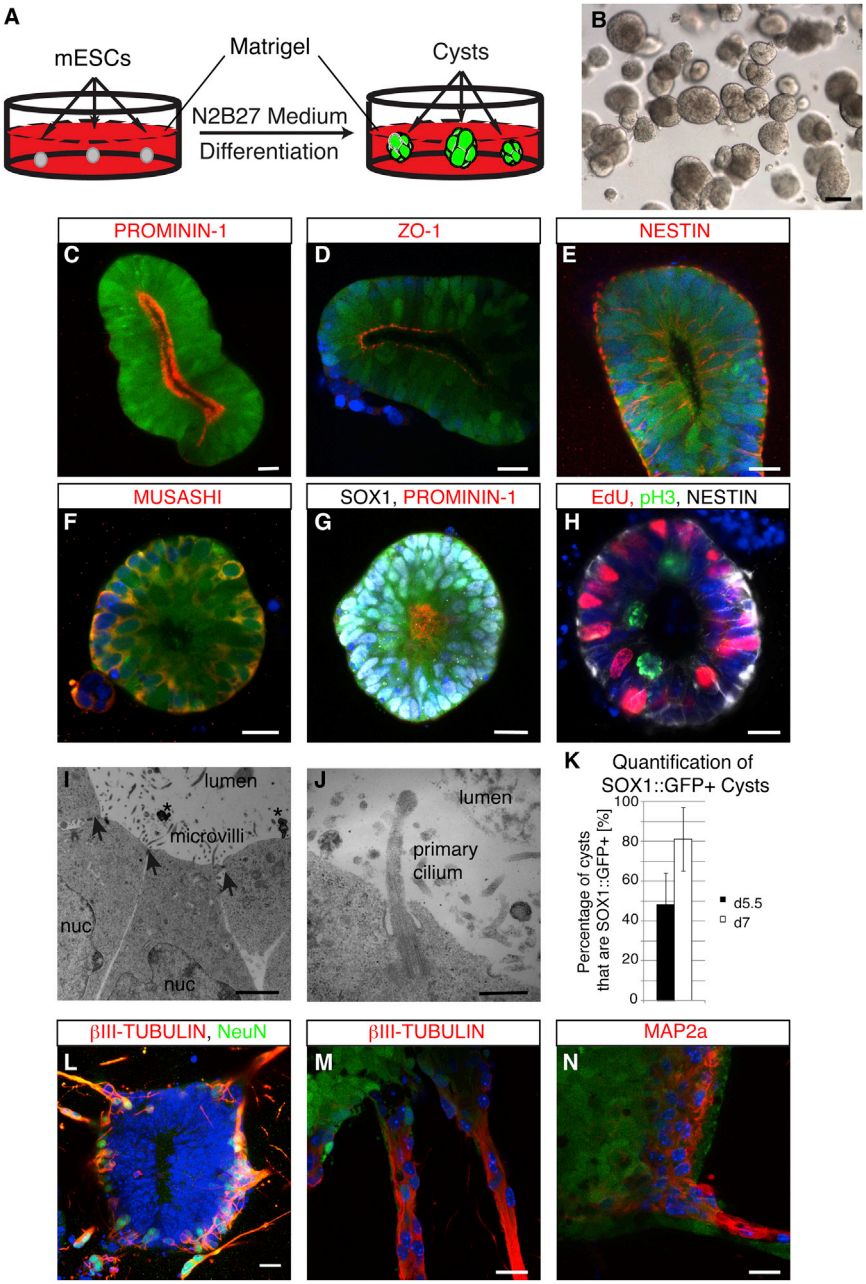

Figure 1. Characterization of Neural Cysts Derived from mESCs

(A–G) Scheme of the generation of neural cysts. Within 5 days neuroepithelial cysts form that express SOX1::GFP and possess a single lumen (B). Day 6 neural cysts are apicobasally polarized, as shown by the luminally expression of PROMININ-1 (C and G) and the tight junction marker ZO-1 (D). The neural stem cell markers NESTIN (E) and MUSASHI (F) are also being expressed. To show that SOX1::GFP cysts are 100% neural in character, we also stained for the protein SOX1 (white nuclei, G).

(H) Cells in a cyst undergo interkinetic nuclear migration, as evidenced by staining for phosphorylated histone 3 (pH3) and the thymidine analog EdU. Cells undergoing division are located at the apical side ($pH3^+$), whereas cells in S phase which are EdU^+ are located at the basal side.

(I and J) Electron microscopic analysis of early neuroepithelial cysts. Cysts possess tight junctions (arrows), have large apical membrane surfaces with microvilli and primary cilia (J), and shed midbodies (stars) into the lumen.

(K) Quantification of $SOX1::GFP^+$ cysts at day 5.5 and day 7 of differentiation. Data are represented as mean ± SD (n = 3 independent experiments with 100 cysts counted per experiment).

(L–N) Around day 7 to day 8, postmitotic neurons start to grow out basally, as evidenced by NeuN (L) and βIII-TUBULIN (L and M) as well as MAP2a (N).

Nuclei were counterstained with Hoechst. All data shown were derived with the SOX1::GFP reporter cell line 46C. All immunofluorescence panels (C–H and L–N) represent confocal images of 3D cysts. Scale bars represent 20 μm (C–H and L–N), 2 μm (I), and 0.5 μm (J). See also Figure S1.

PROMININ-1, ZO-1, and N-CADHERIN (Figures 1C, 1D, 1G, and S1B–S1E). Second, the neural stem cell markers NESTIN and MUSASHI (Figures 1E and 1F) were expressed uniformly. Third, the cells underwent interkinetic nuclear migration reflected by apically localized phospho-histone $H3^+$ ($pH3^+$) mitotic figures and basally localized S-phase nuclei (Figure 1H). Electron microscopy revealed large apical membrane surfaces with microvilli and primary cilia, midbodies, and tight junctions, similar to the ultrastructure of the E8 murine embryonic neural tube (Figures 1I and 1J).

SOX1 expression was used to quantify the percentage of cysts with neuroepithelial identity. On day 5.5, 43.8% ± 16.8% and on day 7 81% ± 4.2% of 46C cysts expressed GFP (Figure 1K). To exclude that the increase in the proportion of $SOX1::GFP^+$ cysts was due to massive cell death, we followed cyst formation and SOX1 expression in live cultures (Figure S2A). A stable number of cysts differentiated over time without significant cell death. Immunostaining showed that many cysts already started to express SOX1::GFP by day 4 (Figure S2B). R1 ESCs formed a similar percentage of $SOX1^+$ cysts by day 6 (Figure S1F).

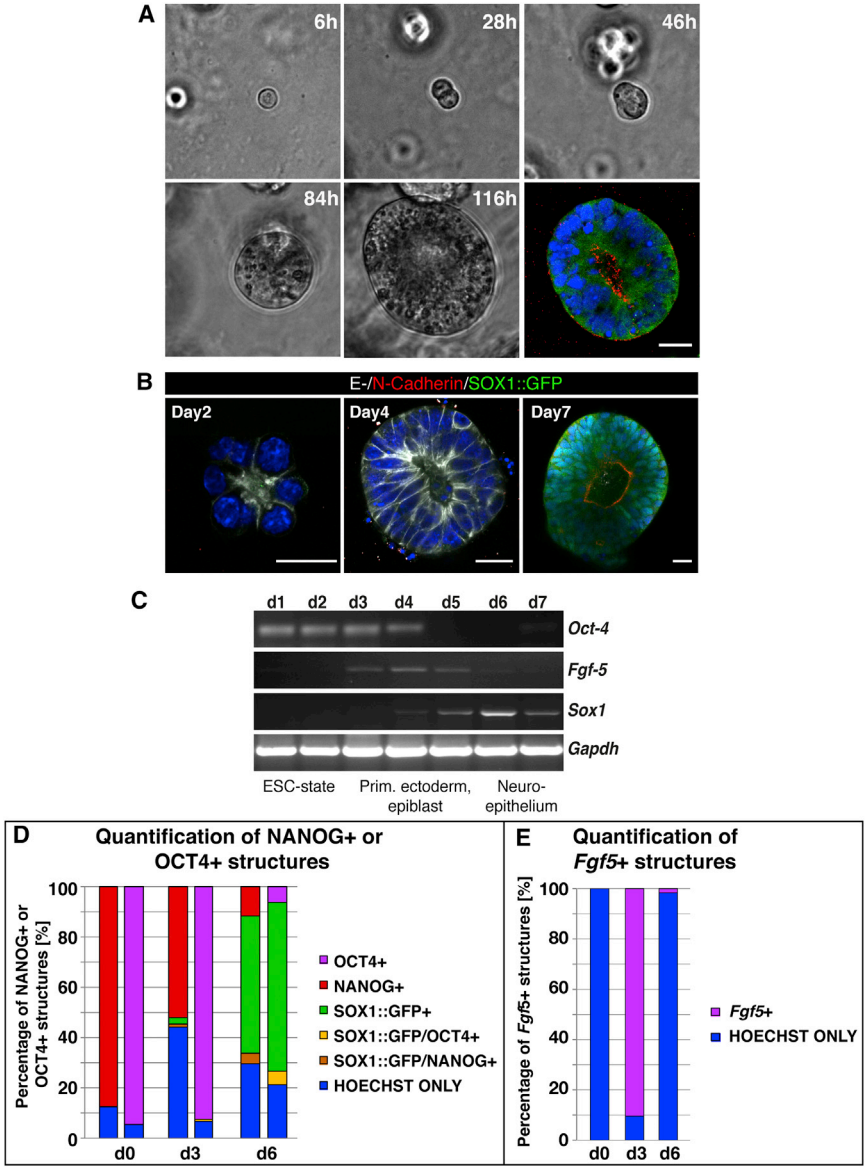

Figure 2. Neural Cysts Can Develop Clonally and Show Progressive Expression of Early Developmental Markers

(A) Phase-contrast images from Movie S1 showing the clonal growth of a neuroepithelial cyst over a time course of 5 days (20×). The imaged cyst was fixed and stained for PROMININ-1 (red) showing that the imaged cyst possesses a lumen.

(B) E-CADHERIN and N-CADHERIN expression during a time course. Early cysts express exclusively E-CADHERIN (days 2–4). By day 7, many cysts express SOX-1 and concomitantly show high N-CADHERIN and low E-CADHERIN expression. Nuclei were counterstained with Hoechst. Scale bars represent 20 μm.

(C–E) RT-PCR analysis for markers that are expressed during early development. From day 0 to day 3, cells exclusively express the ESC marker *Oct4*. Then *Fgf5* starts being expressed, a marker for primitive ectoderm. *Fgf5* becomes downregulated as the neuroectodermal marker *Sox1* starts being expressed. Using immunofluorescence, the progression of developmental markers was quantified in more detail (D; see Figure S3). OCT4 and NANOG were expressed in almost all cells on day 0 after seeding. OCT4 expression persisted up to day 3, whereas NANOG expression declined. On day 6, the majority of the structures analyzed were SOX1$^+$. *Fgf5* expression was analyzed by ISH and peaked on day 3 but was absent from all structures analyzed on day 0 and day 6 (E). Data shown in (D) and (E) represent counts from one out of three representative experiments in which around 1,000 cells on day 0 and 200 cysts on day 3 and day 6 were counted.

See also Figures S2 and S3 and Movie S1.

We next investigated neuronal differentiation. Early neural cysts (5–6 days) were composed solely of SOX1$^+$ cells (Figures 1G and S1B), but around day 7 to day 8, neurons started to grow out basolaterally as detected by NeuN, βIII TUBULIN, and MAP2a (Figures 1L–1N and S1G). At day 9, R1 cysts typically consisted of six layers of pseudostratified progenitors and up to four neuronal cell layers.

Neuroepithelial Cysts Can Initiate Clonally and Show Progressive Expression of Early Developmental Markers

Time-lapse microscopy was used to determine whether cysts can form from single cells. Movie S1 and the associated panels (Figure 2A) show that a single ESC remained in a stable position and clonally formed a neuroepithelial cyst. Whole-mount immunostainings and confocal imaging of PROMININ-1 after time-lapse acquisition showed that clonal neuroepithelial cysts possessed single lumina (Figure 2A). The vast majority of the initial ESC suspension represented single cells, but a minority of two- to three-cell clusters also gave rise to cysts. In addition, filming and the presence of bilobed cysts indicated that closely juxtaposed cysts can fuse at a frequency of 5% or less. We excluded such bilobed cysts from the quantitative analysis.

We next examined the onset of neural commitment using developmental markers. Immunostainings for E- and N-CADHERIN showed that on day 2 and day 4 cysts already harbor a visible lumen and express E-CADHERIN but not

yet N-CADHERIN. Robust N-CADHERIN and SOX1 and loss of E-CADHERIN expression was seen by day 7 (Figure 2B) with significant onset of SOX1 expression starting on day 4 (Figure S2). We also asked whether pluripotent cells progress through a primitive ectoderm-like stage via an expression time course of OCT4, NANOG, and *Fgf-5* by RT-PCR and histological analysis (Figures 2C–2E and S3). *Oct4* was detectable by PCR during the first 4 days, while *Fgf-5* expression appeared from day 3 to day 5 and *Sox1* rising from day 4 to day 6. Immunofluorescence showed that OCT4 was expressed in almost all cells up to day 3 (day 0, 926/979 cells; day 3, 326/354 cysts) (Figures 2D and S3) while about 50% of the cysts downregulated NANOG by day 3 (114/216 cysts). *Fgf-5* expression peaked on day 3 (120/133 cysts) (Figures 2E and S3). A small minority of aggregates that did not possess a lumen and is therefore not called a cyst continued to express OCT4 or NANOG uniformly at day 6 (16/254 $OCT4^+$; 21/183 $NANOG^+$), suggesting the perdurance of some undifferentiated ESCs. A small proportion of cysts coexpressed OCT4 and SOX1 (14/254) or NANOG and SOX1 (8/183) (Figure 2D). These results show that during neural cyst formation, ESCs turn on a marker of primitive ectoderm before differentiating into neurectoderm. The timing of the transitions correlated with murine development. mESCs correspond to E3.5 of mouse development. The onset of *Sox1* expression was detected around day 4 of in vitro differentiation, corresponding to stage E7.5, gastrulation.

Neuroepithelial Cysts Resemble Neural Plate Progenitors and Are Responsive to Morphogens

The neural plate initially consists of multipotent proliferating progenitors that largely express PAX3, PAX7, and MSX1+2 (Briscoe and Ericson, 2001; Jeong and McMahon, 2005; Liem et al., 1995; Peterson et al., 2012). Graded SHH signaling from the midline promotes ventral patterning leading to five distinct progenitor regions (Chamberlain et al., 2008; Jessell, 2000; Nishi et al., 2009; Roelink et al., 1995).

To investigate whether neuroepithelial cysts resemble the neural plate, we assessed dorsal markers. Whole-mount immunostainings revealed that the majority of 46C and R1 cysts uniformly coexpressed PAX3 and PAX7 (Figure 3A; data not shown). *Msx1* and the dorsal signaling molecules *Wnt1* and *Bmp7* were also expressed with some differences among the cell lines (Figures 3B, S4A, and S4B). Exposure of cysts to 1 μM smoothened agonist (SAG) on day 3 for 24 hr yielded cysts that by day 7 had repressed *Msx1* (Figure 3C) but were positive for *Shh* (Figure 3F), FOXA2, and SHH at day 7 (Figure 3H, bottom; data not shown). These results indicate that neuroepithelial cysts can be ventralized to FP.

We did not observe any *Brachyury* expression by RT-PCR or in situ hybridization (ISH) (Figure S4C), suggesting that SAG acted directly on the neuroepithelial cells to induce FP rather than via a notochord intermediate.

Posteriorization Potential of Neural Cysts

We next determined the default anterior/posterior (A/P) positional identity of the neural cysts. 46C and R1 cysts were $Otx2^+$, $Gbx2^+$, $HoxA2^+$, and $Pax6^-$ by RT-PCR (Figures 4A and S5A) indicating an anterior identity. Diencephalon and spinal cord identities were excluded due to a lack of *Pax6* and of *HoxC4*, *HoxC5*, *HoxC6*, and *HoxC8* (Figures 4A and S5A). ISHs (46C and IB10) and immunofluorescence (46C, R1, and IB10) confirmed the PCR results. OTX2 mRNA and protein expression was observed in approximately 50% of 46C and IB10 cysts, whereas it was absent in R1 cysts (Figures 4B–4D, top; Figures S5B and S5C). *Gbx2* expression was found in almost half of cysts, and a small minority of 46C and IB10 cysts showed *HoxC4* and *HoxC6* expression (Figure 4B, top; Figure S5B). No HOXB4 protein expression was observed (Figure 4D, top; Figure S5D, top). Coimmunostaining for OTX2 and EN1, two markers that are coexpressed in the midbrain, showed that all $OTX2^+$ cysts coexpressed EN1, suggesting midbrain identity (Figure 4C; Figure S5C, top).

To posteriorize the cysts, we turned to RA (Okada et al., 2004; Wichterle et al., 2002). The addition of 250 nM RA for 18 hr at day 2 induced posteriorization to cervical levels in 93% of neural cysts, as evidenced by the induction of *HoxC4* and downregulation of *Otx2* (Figures 4A and 4B, bottom; Figure S5A). *HoxC6* expression could be found in a minority of cysts (Figures 4A and 4B, bottom). These data were confirmed by immunostainings for OTX2 and HOXB4 on day 7 (Figure 4D, bottom; Figure S5D, bottom).

Global RA Application Also Induces SHH^+ FP and Consequent D/V Patterning

We next sought to achieve DV patterning in posteriorized cervical cysts via induction of a localized FP. Remarkably, patterning including localized FP formation occurred spontaneously after RA induced posteriorization in 44.1% ± 9.8% of R1 cysts and in 43.7% ± 17% of 46C cysts (Figures 5 and 6A). The great majority of self-patterned cysts only possessed one FP (203/207), while 4 cysts out of 207 had two FPs. RA induced SHH^+ FPs lacked SOX1 (Figure 5A), displayed basally located nuclei (arrow), and coexpressed FOXA2 and ARX with FOXA2 expanding a bit further laterally as seen in the in vivo FP (Figures 5C and S6B). ARX, a late FP marker, was found starting from day 7.

To examine whether FP formation had occurred via RA-induced mesodermal differentiation, we checked patterned cysts via RT-PCR and ISH for *Brachyury* and found no detectable *Brachyury* signal, suggesting that FP induction via RA stimulation is a direct event on neural cells (data not shown).

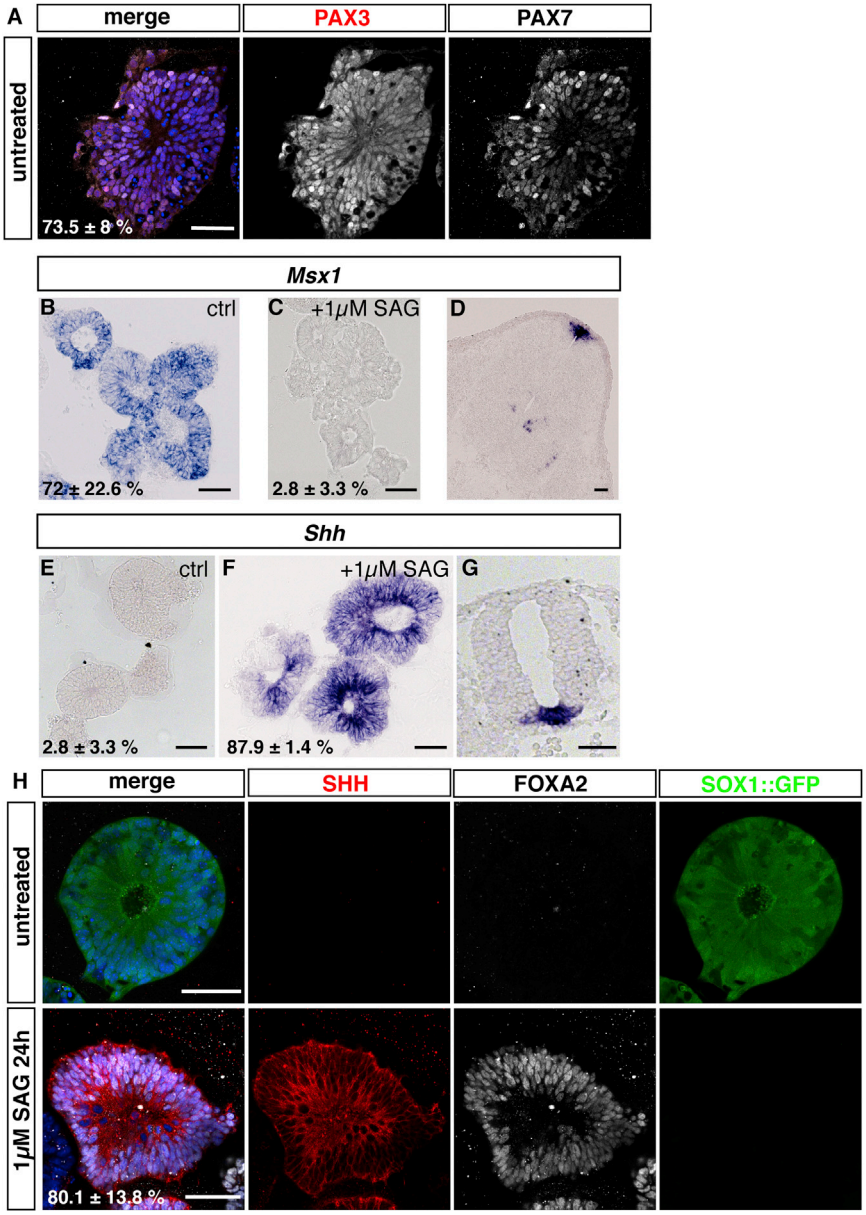

Figure 3. Default Dorsal Identity of Neural Cysts and Their Ventralizability by SHH Signaling

(A) Immunostained neuroepithelial 46C cysts were PAX7$^+$ (white) and PAX3$^+$ (red) showing their dorsal identity. PAX3 expression is shown in black and white in the single stained panel but in red in the merge. SOX1::GFP was not imaged.

(B) Characterization of the DV identity of neuroepithelial cysts by ISH using an *Msx1* probe showing that untreated 46C cysts are *Msx1*$^+$.

(C) After ventralization with 1 μM SAG, cysts do not express *Msx1* anymore.

(D) As corresponding positive control, we used a cross-section of a murine E12.5 spinal cord that shows labeling only at the roof plate.

(E and F) ISH for *shh* to show that untreated 46C cysts are negative for *shh* but express *shh* upon stimulation with 1μM SAG for 24 hr on day 3 (F).

(G) As a corresponding positive control to show the specificity of our probe, we used a cross-section of a murine E9.5 spinal cord that shows labeling only in the FP.

(H) Untreated 46C control cysts express SOX1::GFP and are FOXA2$^-$ as well as SHH$^-$ (top). Addition of 1 μM SAG on day 3 for 24 hr leads to the induction of FOXA2 and SHH while SOX1::GFP gets downregulated, indicating that neural cysts are able to differentiate into FP (bottom).

All nuclei in (A) and (H) were counterstained with Hoechst. Scale bars represent 50 μm (A–H). See also Figure S4.

We next examined the distribution of ventral cell types near the induced FP. The MN marker OLIG2 was expressed close but not adjacent to the SHH$^+$ zone (Figures 5C and 5D), suggesting that intervening regions had p3 identity. ISL1/2, the differentiation marker for MNs, was also found close to the FP distributed laterally (Figure 5E). Neurons grew out of the neuroepithelial cysts on the basolateral sides, as evidenced by βIII-TUBULIN staining (Figure 5E). The interneuron marker LIM1+2 (Figure 5D) was found further from the SHH zone than OLIG2. The dorsal markers PAX3 and BRN3a could both be detected in some of the self-patterned cysts opposite the FP (Figure 5F). To investigate BMP signaling, we immunostained patterned cysts for activated SMADs (pSMAD) and observed nuclear signals opposite to the FP (Figure S6C).

Interestingly, cysts that expressed localized SHH and PAX3 (SHH$^+$/PAX3$^+$) were on average larger (139.3 ± 35 μm) than unpatterned (PAX3$^+$, 97 ± 28 μm) or partially patterned (SHH$^+$, 124.9 ± 38.2 μm) cysts (Figure S6D), suggesting that the full spectrum of DV cell types could only be achieved by large cysts in which cells opposite the FP escaped its signaling. Smaller FP-containing cysts showed a less complete spectrum of dorsal cell types, PAX3$^-$ and BRN3a$^-$, but OLIG2$^+$ and LIM1+2$^+$, suggesting that ventralizing SHH signals had dominated.

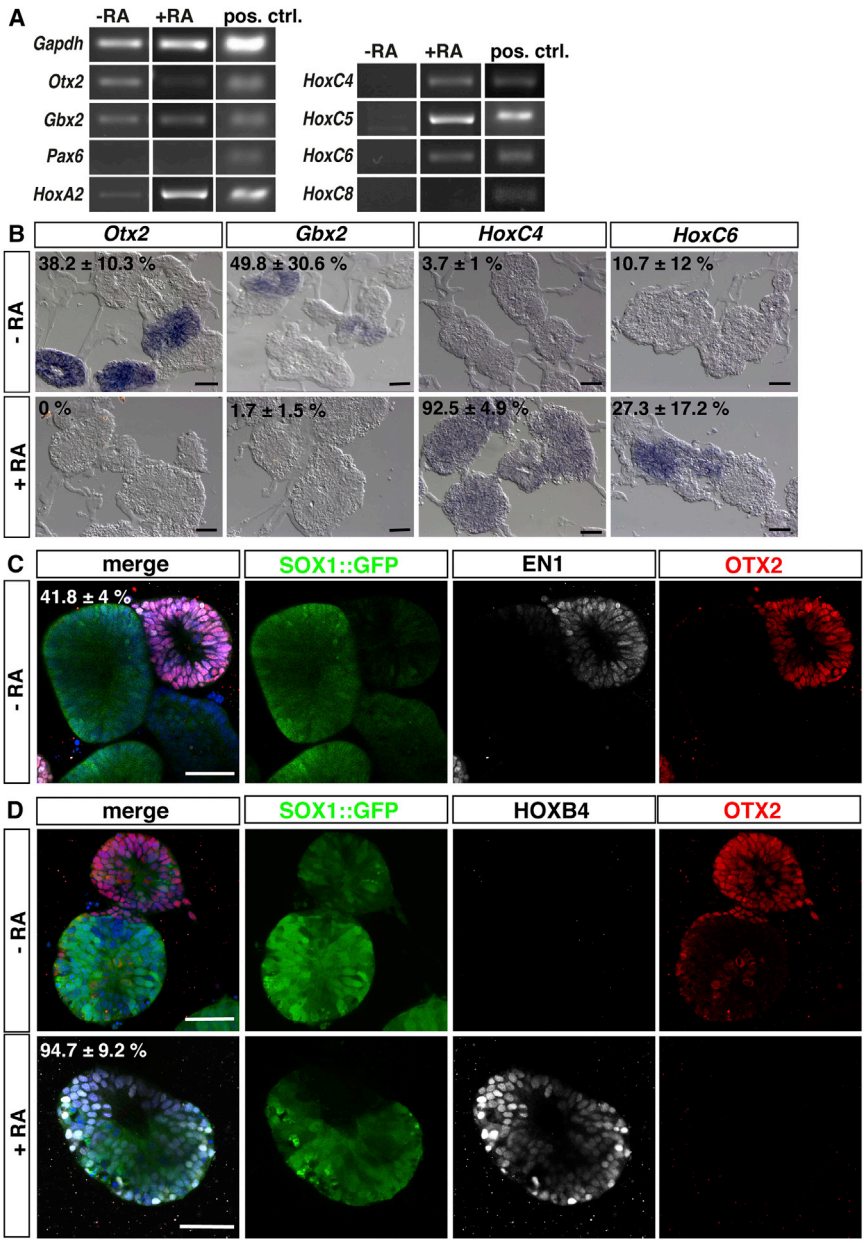

Figure 4. A/P Positional Identity of Neural Cysts and Posteriorization to the Cervical Spinal Cord

(A) RT-PCR analyses for markers of A/P identity using untreated cysts (−RA) as well as posteriorized cysts (+RA) on day 7 of differentiation. As positive control, murine genomic DNA was used.

(B) ISH on cryosectioned cysts to examine localization of *Otx2*, *Gbx2*, *HoxC4* and *HoxC6* mRNAs (top). Subsets of day 7 cysts express *Otx2* or *Gbx2*. Almost all cysts were *HoxC4*$^{-}$ and *HoxC6*$^{-}$. After treating cysts with 250 nM RA for 18 hr, *Otx2* and *Gbx2* are downregulated. *HoxC4* is upregulated in almost all RA treated neural cysts, whereas *HoxC6* is only expressed in a minority of RA treated cysts (bottom).

(C) Immunofluorescence analysis of untreated cysts immunostained for OTX2 (red) and EN1 (white). SOX1::GFP$^{low/-}$ neural cysts coexpress OTX2 and EN1. SOX1-GFP^{+} cysts are negative for both markers.

(D) Immunofluorescence analysis of untreated cysts immunostained for OTX2 (red) and HOXB4 (white) showing that all control cysts are HOXB4^{-} (top). After posteriorization with 250 nM RA for 18 hr on day 2, cysts uniformly express HOXB4, whereas OTX2 is downregulated (bottom). All nuclei in (C) and (D) were counterstained with Hoechst.

Scale bars represent 50 μm (B–D). See also Figure S5.

Since RA is added early (day 2) in our protocol, we strove to define the earliest time point in which a hallmark of patterning could be observed. We stained day 3 to day 7 cysts for OLIG2, SHH, and FOXA2 and called a cyst "patterned" when it expressed OLIG2 and one FP marker at the same time. On day 3, 6% ± 10.4% and on day 4, 42.2% ± 14.9% of R1 cysts expressed FOXA2 (Figure 6B) but did not yet express any OLIG2 or SHH. On day 5, 17.5% ± 9% of the cysts were FOXA2^{+} but still OLIG2^{-} and SHH^{-}, and 17.6% ± 6.0% of all cysts expressed OLIG2 as well as FOXA2 and SHH and thus were patterned. Only a small population of cysts expressed FOXA2 and SHH but not yet OLIG2. On days 6 and 7, the FOXA2 single-positive population as well as the FOXA2^{+}, SHH^{+},OLIG2^{-} population decreased further whereas the FOXA2^{+},SHH^{+},OLIG2^{+} triple-positive population increased up to 37.7% ± 9%. We conclude that RA stimulation first induces FOXA2 and then SHH expression. Secretion of SHH from the induced source then signals the formation of other ventral cell types like OLIG2^{+} cells nearby.

To directly address whether FP induction can be inhibited, we blocked SHH signaling using cyclopamine that was kept in the culture media either for the duration of the RA pulse (18 hr) or for a total of 72 or 120 hr. The cells were fixed at day 7 and analyzed for FOXA2 and SHH expression. Administration of cyclopamine for 18 hr

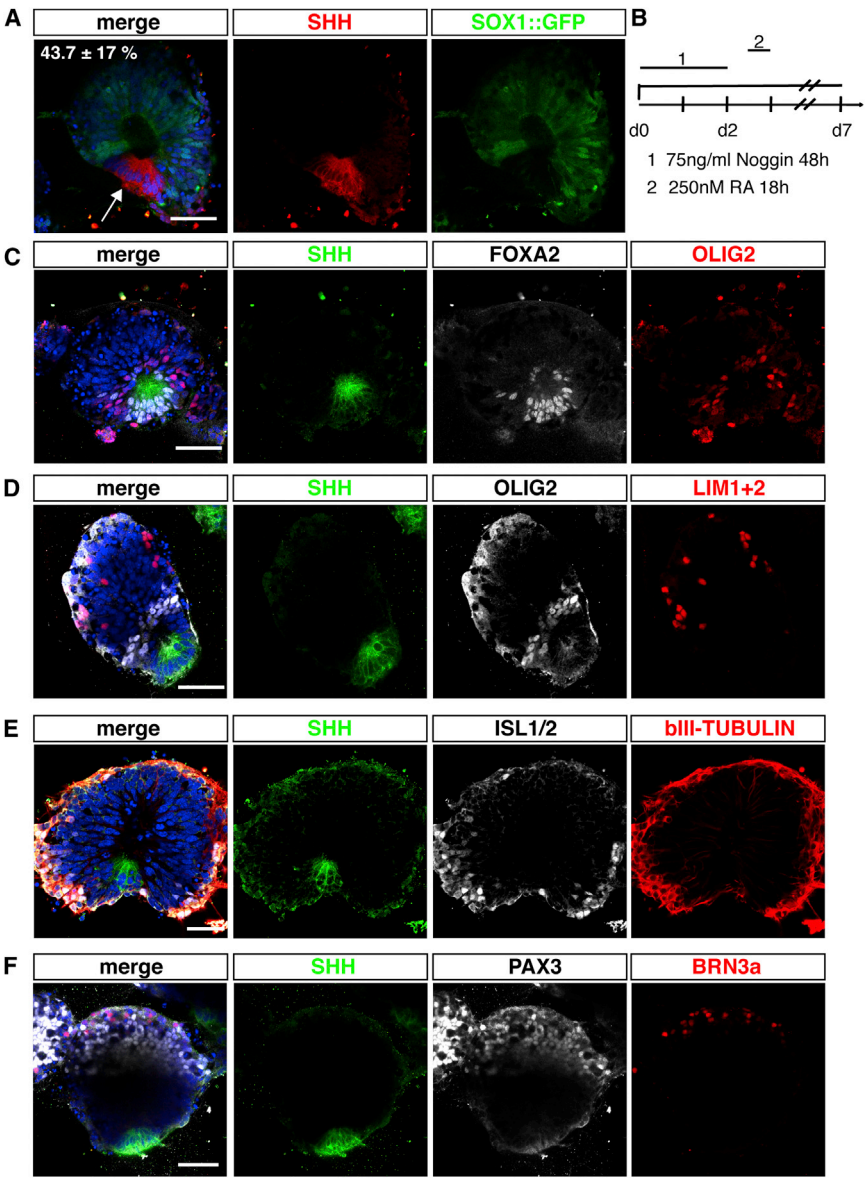

Figure 5. Self-Organized DV Patterning in Posteriorized Neuroepithelial Cysts

(A) Self-patterned neuroepithelial cysts derived from 46C ESCs show that the FP region which is SHH$^+$ (red) is SOX1::GFP$^-$ and has basally localized nuclei (arrow).

(B) Scheme of the experimental setup.

(C) The FP region coexpresses SHH (green) and FOXA2 (white). Close to the FP region but not directly adjacent to it the progenitor marker OLIG2 (red) stains on both sides, corresponding to the pMN region.

(D) The FP is marked by SHH expression (green) and the pMN region in white by OLIG2 expression. Further dorsal the interneuronal marker LIM1+2 (red) can be detected.

(E) MNs identified by ISL1/2 stainings (white) can be detected close to the FP region stained with SHH (green) as well as dorsally. βIII-TUBULIN immunostaining (red) shows peripheral arrangement of differentiated neurons and their axons.

(F) PAX3 (white) as a general dorsal marker and BRN3a (red) as a differentiation marker for dorsal interneurons were the furthest dorsal markers detected in self-patterned cysts. The FP region is marked in green by SHH.

All nuclei were counterstained with Hoechst. Scale bars represent 50 μm. See also Figure S6.

showed almost no effect on blocking FP formation. Prolonging the cyclopamine treatment to 72 hr significantly reduced the number of cysts harboring a FP (Figure 6C). Only a minority of cysts expressed FOXA2 and SHH when the treatment was prolonged to 120 hr. These results suggest that SHH signaling is necessary in order to induce full FP formation in cysts.

To further show the relevance of SHH signaling on cyst patterning, we incubated the RA-treated cysts with 1 μM SAG on day 3 and found a strong bias to ventral fates. A 9 hr SAG pulse gave rise to SOX1::GFP$^+$ cysts with low levels of FOXA2, strong NKX6.1, as well as NKX2.2 and ISL1/2 but no LIM1+2 (Figure S7A). Lowering SAG to 100 nM for 8 hr yielded a mixture of PAX6$^+$, EVX1/2$^+$ cysts and OLIG2$^+$, LIM1+2$^+$, ISL1/2$^+$ cysts, reflecting more dorsal/lateral fates (Figure S7B).

Defined 3D Matrices Also Permit RA-Induced Self-Patterning

Matrigel is a complex, undefined matrix, so we determined whether cyst formation and RA induced self-patterning also occurred in simpler matrix conditions. We grew R1 cysts in laminin/entactin gels and also found that cysts were uniformly PAX3$^+$ and did not express SHH (Figure 7A). After an RA pulse, 46.8% ± 7.6% of R1 cysts expressed SHH, and we found patterned cysts that expressed PAX3 and BRN3a, as well as OLIG2, and LIM1+2 closer to the SHH$^+$ domain (Figures 7B–7D). To test whether ECM proteins

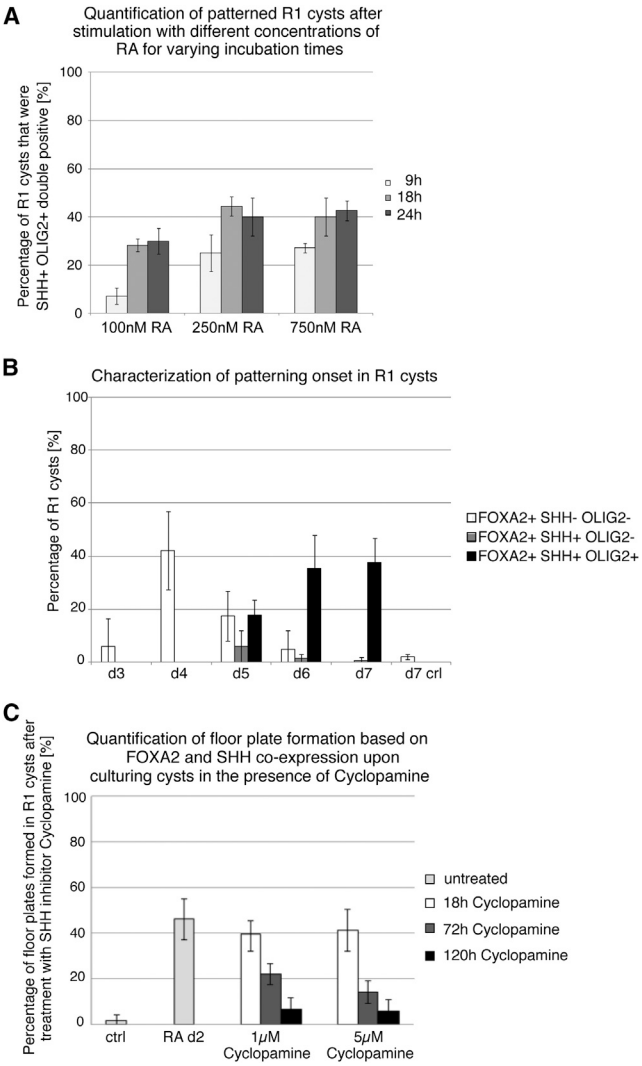

Figure 6. Characterization of FP Induction by RA

(A) Quantification of patterned cysts after stimulation with 100, 250, and 750 nM RA for 9, 18, and 24 hr. R1 cysts were analyzed on day 7 by immunostaining for SHH and OLIG2, and the percentage of cysts that were double positive was determined. Nine hours of incubation with 100 nM RA led to the formation of 7.2% ± 3.3% of self-patterned R1 cysts. This number increased significantly when the incubation period was prolonged to 18 hr (28.3% ± 7.6%) or 24 hr (30% ± 2%). The total fraction of patterned cervical cysts at 100 nM RA irrespective of incubation length never reached the same percentage as that obtained with 250 or 750 nM RA. Incubation with 250 or 750 nM RA led to similar results at any time point investigated (9 hr incubation, 25% ± 2.6% at 250 nM RA; 27.1% ± 5.4% at 750 nM RA; 18 hr or 24 hr incubation, around 40% of patterned cysts). These results indicate that optimal cyst patterning is dependent on a certain RA concentration and incubation time.

(B) Characterization of the patterning onset in R1 cysts. Days 4–7 cysts were stained for OLIG2, FOXA2, and SHH after RA application on day 2, and the percentage of R1 cysts that was positive for any combination of the 3 markers, notably FOXA2$^+$ SHH$^-$ OLIG2$^-$; FOXA2$^+$ SHH$^+$ OLIG2$^-$ and FOXA2$^+$ SHH$^+$ OLIG2$^+$, was determined.

(C) Inhibition of FP induction through the administration of the SHH signaling inhibitor cyclopamine. On day 2, 1 and 5 μM cyclopamine was added together with RA for 18, 72, or 120 hr to growing cysts. On day 7, the percentage of patterned cysts based on the coexpression of FOXA2 and SHH was determined. FP induction was almost completely inhibited when cysts were grown for 120 hr in 1 or 5 μM cyclopamine.

Data are represented as mean ± SD (n = 3 independent experiments with 100 cysts counted per experiment). See also Figure S7.

were necessary at all, we employed pure PEG gels and found patterned cysts at a lower frequency compared with Matrigel conditions (Figure 7E). Complete DV patterned cysts based on PAX3 and SHH expression were also observed (Figures 7F and 7G). These results show that patterning induced by RA is neither dependent on ECM proteins nor on growth factors present in Matrigel.

DISCUSSION

Here we show that single-cell suspensions of mouse ESCs grown in neural differentiation media and 3D matrices form spherical/ellipsoid neuroepithelia that harbor a single lumen, have clear apical/basolateral polarity, and show pseudostratification and interkinetic nuclear migration, structures that we call neuroepithelial cysts. In vivo, the neural tube forms from a planar neuroepithelial sheet that folds together to generate the lumen-containing tube. It is interesting that in vitro, as the ESCs divide and progress along the neural lineage, they generate a lumen at quite early stages corresponding to primitive ectoderm, presumably due to their E-CADHERIN-based epithelial character. This mode of lumen formation may resemble the tendency of inner cell mass cells to generate in vivo rosettes (Bedzhov and Zernicka-Goetz, 2014). Once lumen formation is initiated, it is maintained as the cells transit into an N-CADHERIN$^+$,SOX1$^+$ neuroepithelial state. Upon prolonged culturing, cells within the cysts undergo neural differentiation as judged by expression of transcription factors associated with neuronal precursors, as well as neuronal differentiation markers. The spatial location of the neuronal differentiation occurred at the basal side of the neuroepithelium.

In this system, exogenous extracellular matrix components may have enhanced cyst-forming ability but were not absolutely necessary for lumen-containing neuroepithelial cyst formation, as they also formed in pure PEG gels. Here we implemented relatively high cell densities in the starting culture conditions leading to the possibility of paracrine effects on ECM secretion that might promote cyst formation. Separate work examining cyst formation

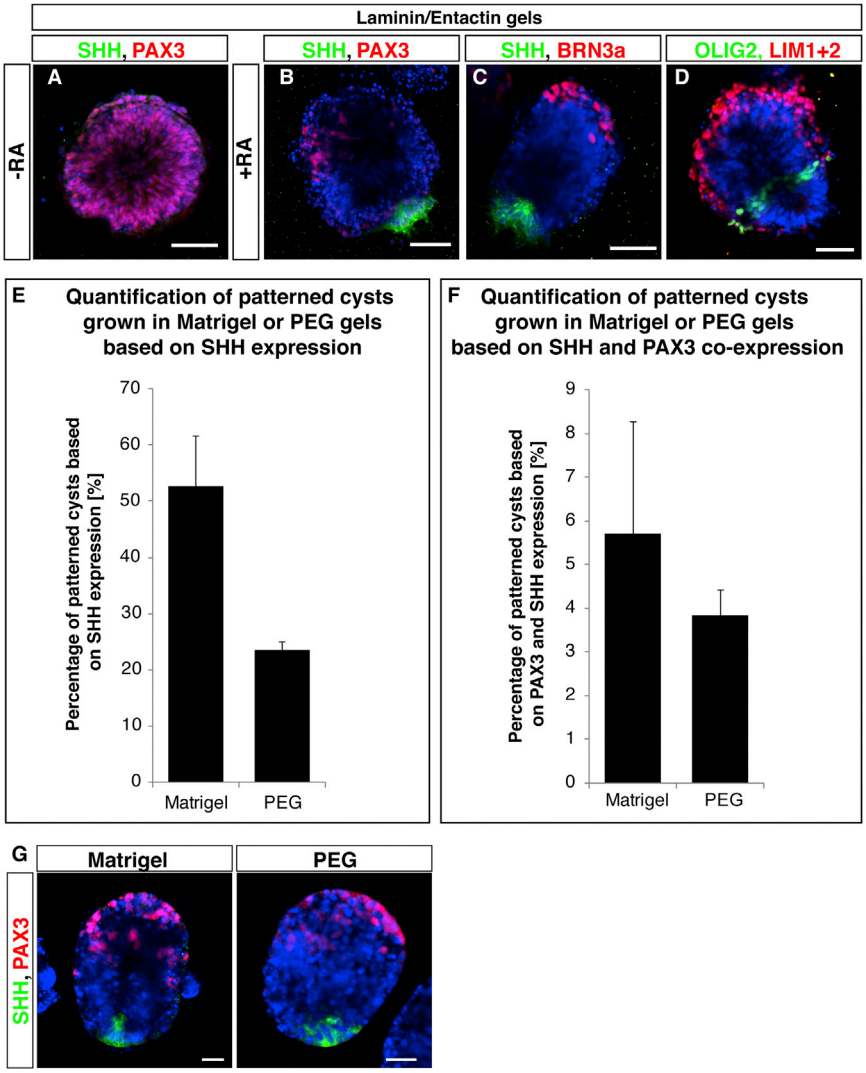

Figure 7. Defined 3D Matrices Also Permit RA-Induced Self-Patterning of Neuroepithelial Cysts

(A–D) Cysts were grown in high concentration laminin/entactin gels. Untreated control cysts were uniformly PAX3$^+$ (red, A) and patterned similar to cysts grown in Matrigel upon a RA pulse on day 2 as evidenced by immunofluorescence staining for SHH (green) and PAX3 (red, B), SHH (green) and BRN3a (red, C) as well as OLIG2 (green) and LIM1+2 (red, D).

(E) Even in pure PEG gels, cysts grew and patterned after RA administration based on focal SHH expression, although to a lesser extent than in Matrigel as quantified.

(F and G) Complete DV patterned cysts based on coexpression of PAX3 and SHH were also observed. Data are represented as mean ± SD for Matrigel (n = 3 independent experiments) and mean ± variance for PEG gels (n = 2 independent experiments) with 100 cysts counted per experiment. Nuclei were counterstained with Hoechst.

Scale bars represent 50 μm (A–D) and 20 μm (G).

under lower density conditions in defined, engineered matrices coupled to proteinaceous ECM components and combined with the soluble factor screening revealed a requirement for paracrine factors and a stronger dependence on matrix components for efficient cyst formation, as well as a stiffness optimum (A.R., unpublished data). Such work will help to define the minimum conditions required to generate neural cysts in the complete isolation from other cells.

Interestingly, we observed localized FP formation after global application of RA and subsequent elaboration of DV progenitor cell domains. Previous work extensively characterizing RA effects on embryoid bodies had shown the induction of SHH by RA administration and consequently the ventralization of neural tube markers (Okada et al., 2004). In those pioneering studies, since the embryoid bodies contained multiple other cell types including mesoderm and the analysis was performed by RT-PCR, it was not clear if the RA was inducing SHH expression in notochord-like cells and/or whether it had induced a FP. The spatial arrangement of the FP and other neural markers could not be analyzed since the immunostaining was performed on replated cells, whereas here we analyze the 3D cysts in situ by confocal microscopy. Since we produce cysts by direct culturing of single ESCs in Matrigel plus neural induction media without serum, we do not find evidence for mesoderm. Through immunostaining, we observed the formation of SHH$^+$ARX$^+$ region within the neuroepithelial cells themselves. These data indicate that our cysts induce a FP that might be directly induced by RA in the absence of induction from a notochord-like structure. We then observe the formation of ventral progenitor domains with a very similar spatial arrangement as that found in the in vivo neural tube (Balaskas et al., 2012).

This observation leads to two questions: first, is RA an endogenous contributor to FP induction, and second,

how does global application lead to the formation of a local FP? The induction of a focal SHH signaling center by RA has been observed in multiple embryological contexts, including chicken wing (Tickle, 1991), zebrafish pectoral fin, and mouse limb (Grandel et al., 2002; Niederreither et al., 1999), incisor (Kronmiller et al., 1995), lung (Desai et al., 2004, 2006), pancreas (Martín et al., 2005), and prostate (Vezina et al., 2008). While SHH from the notochord is required for SHH induction in the neural tube, other molecules are likely to be involved in FP induction. For example, it is not fully explained why the contact of the notochord with the presumptive FP is necessary for induction. Indeed, RA was examined as one potential candidate to cooperate with SHH to induce FP but did not induce SHH in rat neural plate tissue (Placzek et al., 1993). Chick neural plate explants treated with 9-*cis*-RA or RAR agonist did not induce SHH but rather differentiated into NeuroM$^+$ cells (Diez del Corral et al., 2003). However, in these studies, the timing of RA addition may have been too late as cells were already specified to neural fate. In our system, RA was added at day 2 corresponding to gastrulation stage E5.5. Support for an endogenous role for RA in FP induction comes from experiments with *RALDH2*$^{-/-}$ mice. Although the mRNA transcript for *Shh* can be detected at 14–15 somite stage and E9.5, no SHH protein was observed (Ribes et al., 2009). Furthermore Henson's node, notochord, and FP secrete RA (Wagner et al., 1990). Since the nature of the earliest events affecting DV patterning of the neural tube remain obscure, it remains possible that RA signaling during gastrulation/early neurulation contributes to neural tube DV patterning (Sasai and De Robertis, 1997). In vivo, RA may act as a permissive factor that makes the neural plate cells competent to initiate FP formation when the final SHH trigger occurs.

The in vitro conditions for RA-induced FP induction required high concentrations of RA, pointing possibly to an epiphenomenon that jump starts a self-enhancing activator/inhibitor signaling system, leading to localized FP formation. Both the *FoxA2* gene, a transcription factor required for SHH expression, and the *Shh* gene encoding SHH, which can induce FOXA2 expression, have RAR binding elements in their promoters (Chang et al., 1997; Okada et al., 2004). High levels of RA could access these promoters and initiate a positive feedback loop, enhancing expression of SHH. The SHH signaling pathway has a number of negative regulators, including PTC and GLI that could help to establish localized SHH expression (Nishi et al., 2009).

While the neuroepithelial cysts will be a valuable system for the study of patterning and other organizational aspects of neural development, they may ultimately prove valuable as a cell source for regenerative medicine approaches. In this regard, generation of spinal cord neuroepithelial cysts from human pluripotent stem cells would be of interest. Zhu et al. (2013) showed that human ESCs could form neuroepithelial cysts under similar conditions, although the default A/P identity of the cysts was in the eyefield. An important future endeavor will be to define whether RA can simultaneously posteriorize and induce FP in human ESC-derived cysts, as they do in the mouse system.

EXPERIMENTAL PROCEDURES

Differentiation of mESCs in the Neuroepithelial Cyst Model

A mouse Sox1::GFP reporter ESC line (46C, gift of Konstantinos Anastasiadis, BIOTEC TU-Dresden, with permission of Austin Smith, University of Cambridge), R1 mESCs (gift of Ezio Bonifacio, CRTD), and IB10 mESCs (gift of Ronald Naumann, MPI-CBG) were cultured under standard conditions in complete medium consisting of Dulbecco's modified Eagle's medium (GIBCO) containing 15% fetal calf serum (PAA), 2 mM L-glutamine (GIBCO), nonessential amino acids (GIBCO), 1 mM sodium pyruvate, penicillin/streptomycin (Invitrogen), 0.1 mM β-mercaptoethanol (Sigma), and 1,000 U/ml leukemia inhibitory factor (LIF; Chemicon). The medium was changed daily. Every other day cells were passaged by trituration of the colonies after trypsinization. For cyst preparations, single ESCs were washed twice with PBS and resuspended in neural induction medium N2B27 (Pollard et al., 2006). A total of 50,000 single ESCs resuspended in 10 μl N2B27 were embedded in 150 μl Matrigel and distributed equally over five 3.5 cm^2 glass bottom dishes (MatTek). After gelling at 37°C for 15 min, the embedded cells were cultured in N2B27. In separate experiments, laminin/entactin gels (Corning), diluted with chilled N2B27 to 10 mg/ml, or PEG gels (see below) were used instead of Matrigel. The laminin/entactin matrix was allowed to gel for 30 min at 37°C. For posteriorization, 250 nM all-*trans* RA (Sigma) was added to the differentiation medium on day 2 for 18 hr. For ventralization to FP, 1 μM smoothened agonist SAG (Calbiochem) was added on day 3 for 24 hr. To inhibit FP formation, 1 μM or 5 μM cyclopamine (Tocris) was added on day 2 for 18, 72, or 120 hr to the culture medium. The medium was replaced with fresh cyclopamine after the RA pulse (day 3) and on day 5 of cyst growth.

Hydrogel Precursor Synthesis

Forty kDa, 8-arm PEG vinylsulfone (PEG-VS) (NOF) was functionalized with FXIIIa-peptide substrates via Michael-type addition. A glutamine-containing peptide (NQEQVSPL-ERCG-NH_2) and a lysine-containing peptide with an MMP-insensitive sequence (AcFKGG-*GDQGIAGF*-ERCG-NH_2) were used to obtain glutamine-PEG precursor (Q-PEG) and lysine-PEG precursor (A-PEG) polymers. Functionalization and characterization of these precursors were performed as described elsewhere (Ehrbar et al., 2007).

FXIII Activation

Factor XIII (Fibrogammin P, CSL Behring) was reconstituted in water from lyophilized powder to a concentration of 200 U/ml; 1 ml of factor XIIIa was activated with 100 μl of thrombin (20 U/ml; Sigma-Aldrich) for 30 min at 37°C and stored at −80°C for further use.

Hydrogel Preparation

Precursor solutions to give hydrogels with a final dry mass content of 1.5% w/v were prepared by stoichiometrically balanced solutions of Q-PEG and A-PEG in Tris-Buffer (50 mM final concentration [pH 7.6]) containing 50 mM $CaCl_2$. A total of 50,000 ESCs (5 × 10^6 cells/ml) were added to a final gel volume of 150 µl. Crosslinking was initiated by 10 U/ml thrombin-activated factor XIIIa and vigorous mixing. The cell-gel solution was distributed equally over five 35 mm glass bottom culture dishes (MatTek) and gelled for 25 min at 37°C, and the embedded cells were cultured in N2B27 identical to Matrigel culture.

Immunocytochemistry

Whole-mount preparations were fixed in 4% paraformaldehyde (Sigma Aldrich) for 20 min at room temperature. After quenching (1 × PBS, 200 mM glycine, 0.3% Triton X-100) and antigen retrieval (70°C, 25 min, 1 × citrate buffer; DAKO), the tissue was blocked for 1 hr at room temperature (1 × PBS, 0.5% BSA, 0.3% Triton X-100). Immunostaining was performed in blocking buffer at 4°C overnight. The list of primary and secondary antibodies can be found in the Supplemental Experimental Procedures.

For 5-ethynyl-2′-deoxyuridine (EdU) incorporation, day 5 neural cysts were incubated with EdU for 1 hr and fixed thereafter. EdU was detected using the Click-iT EdU Alexa Fluor 647 Imaging Kit (Invitrogen).

For the pSMAD, SHH double staining, cysts were first stained for pSMAD, and after several washes, SHH staining was performed on top. Negative controls were performed using either no primary antibody or lambda protein phosphatase (New England Biolabs) treatment.

Fluorescent images were collected using a Leica TCS SPE or Zeiss LSM 510 confocal microscope. Acquisition was 2-fold oversampled, and pictures blurred afterward.

Time-Lapse Analysis

Cyst formation was imaged through the acquisition of z stacks every 2 hr using MetaMorph Software using a motorized inverted Zeiss microscope that was temperature and CO_2 controlled. SOX1::GFP cyst tracking from day 2 to day 6 was performed using a Zeiss Axio Observer system. Six positions per dish were saved and reimaged on a daily routine.

RT-PCR

Total RNA was extracted from untreated or posteriorized mESC derived cysts using an RNeasy kit (QIAGEN), treated with RNase-free DNaseI (Invitrogen), and reverse transcribed with SuperScript II (Invitrogen). The synthesized cDNA was amplified with gene-specific primers. The primers used are available in the Supplemental Experimental Procedures.

ISH on Cyst Cryosections

ISHs were carried out on 12 µm cryosections as previously described (Schnapp et al., 2005; Zhu et al., 2013). Sense and antisense probes of *Otx2*, *Gbx2*, *HoxC4*, *HoxC6*, *Shh*, *Bmp7*, *Fgf5*, and *Msx1* for ISHs were obtained by PCR from murine genomic DNA. An antisense probe for *Brachyury* was obtained by PCR from murine E13 cDNA, and the antisense probe for *Wnt1* was obtained by PCR from the clone D030017M24. The primers used for probe generation as well as a detailed protocol are available in the Supplemental Experimental Procedures.

Electron Microscopy

Electron microscopy analysis was performed as described (Dubreuil et al., 2007). A more detailed description can be found in the Supplemental Experimental Procedures.

Statistical Analysis

Values are expressed as mean ± SD. All experiments were repeated at least three times except the characterization of IB10 (n = 2). For quantification of immunostained cysts, 100 cysts were manually counted per dish in random fields from confocal microscope images based on Hoechst-stained nuclei and their morphological appearance to determine the total number of cysts. For quantifications of unpatterned cysts, we counted a cyst as positive for a specific marker when this marker was expressed in about 50% of the cells. In self-patterned cysts, we counted cysts as patterned and positive for a specific marker as soon as we could detect a few positive cells. For quantification of ISHs, 200 to 500 cysts were counted manually.

SUPPLEMENTAL INFORMATION

Supplemental Information includes Supplemental Experimental Procedures, seven figures, and one movie and can be found with this article online at http://dx.doi.org/10.1016/j.stemcr.2014.09.020.

AUTHOR CONTRIBUTIONS

A.M. and E.M.T. designed and analyzed most of the experiments, and A.M. performed most of the experiments. D.E. helped to characterize the culture system in more detail. A.T. prepared probes for ISH, performed ISH, and analyzed it. M.N. and A.S. helped with the generation of probes for ISH and the DV characterization of the cysts. A.R., D.E., and M.L. contributed 3D experiments in PEG gels. G.S and E.M.T. provided funding for the work. A.M. and E.M.T. wrote the manuscript.

ACKNOWLEDGMENTS

We thank Konstantinos Anastassiadis for the mouse ESC line 46C that we received with permission from Austin Smith, Ezio Bonifacio for the R1 mouse ESC line, Ronald Naumann for the IB10 mouse ESC line, Hideyuki Okano for the anti-MUSASHI antibody, David Drechsel and Ines Wagner for the human Noggin-Fc, Tatiana Sandoval-Guzman for embryonic mouse sections, Regina Wegner for mESCs and cyst cultures, and Wieland Huttner for the anti-PROMININ-1 antibody as well as for his support for electron microscopy analysis. This work was supported by a seed grant and core support from the DFG-Research Center of Regenerative Therapies Dresden, the International Foundation for Paraplegia, and the Saw-2011-IPF-2 68 grant of the Leibniz Society.

Received: August 21, 2014
Revised: September 28, 2014
Accepted: September 29, 2014
Published: October 30, 2014

REFERENCES

Antonica, F., Kasprzyk, D.F., Opitz, R., Iacovino, M., Liao, X.H., Dumitrescu, A.M., Refetoff, S., Peremans, K., Manto, M., Kyba, M., and Costagliola, S. (2012). Generation of functional thyroid from embryonic stem cells. Nature *491*, 66–71.

Aubert, J., Stavridis, M.P., Tweedie, S., O'Reilly, M., Vierlinger, K., Li, M., Ghazal, P., Pratt, T., Mason, J.O., Roy, D., and Smith, A. (2003). Screening for mammalian neural genes via fluorescence-activated cell sorter purification of neural precursors from Sox1-gfp knock-in mice. Proc. Natl. Acad. Sci. USA *100* (*Suppl 1*), 11836–11841.

Balaskas, N., Ribeiro, A., Panovska, J., Dessaud, E., Sasai, N., Page, K.M., Briscoe, J., and Ribes, V. (2012). Gene regulatory logic for reading the Sonic Hedgehog signaling gradient in the vertebrate neural tube. Cell *148*, 273–284.

Bedzhov, I., and Zernicka-Goetz, M. (2014). Self-organizing properties of mouse pluripotent cells initiate morphogenesis upon implantation. Cell *156*, 1032–1044.

Briscoe, J., and Ericson, J. (2001). Specification of neuronal fates in the ventral neural tube. Curr. Opin. Neurobiol. *11*, 43–49.

Chamberlain, C.E., Jeong, J., Guo, C., Allen, B.L., and McMahon, A.P. (2008). Notochord-derived Shh concentrates in close association with the apically positioned basal body in neural target cells and forms a dynamic gradient during neural patterning. Development *135*, 1097–1106.

Chang, B.E., Blader, P., Fischer, N., Ingham, P.W., and Strähle, U. (1997). Axial (HNF3beta) and retinoic acid receptors are regulators of the zebrafish sonic hedgehog promoter. EMBO J. *16*, 3955–3964.

Desai, T.J., Malpel, S., Flentke, G.R., Smith, S.M., and Cardoso, W.V. (2004). Retinoic acid selectively regulates Fgf10 expression and maintains cell identity in the prospective lung field of the developing foregut. Dev. Biol. *273*, 402–415.

Desai, T.J., Chen, F., Lü, J., Qian, J., Niederreither, K., Dollé, P., Chambon, P., and Cardoso, W.V. (2006). Distinct roles for retinoic acid receptors alpha and beta in early lung morphogenesis. Dev. Biol. *291*, 12–24.

Diez del Corral, R., Olivera-Martinez, I., Goriely, A., Gale, E., Maden, M., and Storey, K. (2003). Opposing FGF and retinoid pathways control ventral neural pattern, neuronal differentiation, and segmentation during body axis extension. Neuron *40*, 65–79.

Dubreuil, V., Marzesco, A.M., Corbeil, D., Huttner, W.B., and Wilsch-Bräuninger, M. (2007). Midbody and primary cilium of neural progenitors release extracellular membrane particles enriched in the stem cell marker prominin-1. J. Cell Biol. *176*, 483–495.

Ehrbar, M., Rizzi, S.C., Schoenmakers, R.G., Miguel, B.S., Hubbell, J.A., Weber, F.E., and Lutolf, M.P. (2007). Biomolecular hydrogels formed and degraded via site-specific enzymatic reactions. Biomacromolecules *8*, 3000–3007.

Eiraku, M., Watanabe, K., Matsuo-Takasaki, M., Kawada, M., Yonemura, S., Matsumura, M., Wataya, T., Nishiyama, A., Muguruma, K., and Sasai, Y. (2008). Self-organized formation of polarized cortical tissues from ESCs and its active manipulation by extrinsic signals. Cell Stem Cell *3*, 519–532.

Eiraku, M., Takata, N., Ishibashi, H., Kawada, M., Sakakura, E., Okuda, S., Sekiguchi, K., Adachi, T., and Sasai, Y. (2011). Self-organizing optic-cup morphogenesis in three-dimensional culture. Nature *472*, 51–56.

Elkabetz, Y., Panagiotakos, G., Al Shamy, G., Socci, N.D., Tabar, V., and Studer, L. (2008). Human ES cell-derived neural rosettes reveal a functionally distinct early neural stem cell stage. Genes Dev. *22*, 152–165.

Grandel, H., Lun, K., Rauch, G.J., Rhinn, M., Piotrowski, T., Houart, C., Sordino, P., Küchler, A.M., Schulte-Merker, S., Geisler, R., et al. (2002). Retinoic acid signalling in the zebrafish embryo is necessary during pre-segmentation stages to pattern the anterior-posterior axis of the CNS and to induce a pectoral fin bud. Development *129*, 2851–2865.

Huch, M., Dorrell, C., Boj, S.F., van Es, J.H., Li, V.S., van de Wetering, M., Sato, T., Hamer, K., Sasaki, N., Finegold, M.J., et al. (2013). In vitro expansion of single Lgr5+ liver stem cells induced by Wnt-driven regeneration. Nature *494*, 247–250.

Jeong, J., and McMahon, A.P. (2005). Growth and pattern of the mammalian neural tube are governed by partially overlapping feedback activities of the hedgehog antagonists patched 1 and Hhip1. Development *132*, 143–154.

Jessell, T.M. (2000). Neuronal specification in the spinal cord: inductive signals and transcriptional codes. Nat. Rev. Genet. *1*, 20–29.

Kronmiller, J.E., Nguyen, T., and Berndt, W. (1995). Instruction by retinoic acid of incisor morphology in the mouse embryonic mandible. Arch. Oral Biol. *40*, 589–595.

Lazzari, G., Colleoni, S., Giannelli, S.G., Brunetti, D., Colombo, E., Lagutina, I., Galli, C., and Broccoli, V. (2006). Direct derivation of neural rosettes from cloned bovine blastocysts: a model of early neurulation events and neural crest specification in vitro. Stem Cells *24*, 2514–2521.

Liem, K.F., Jr., Tremml, G., Roelink, H., and Jessell, T.M. (1995). Dorsal differentiation of neural plate cells induced by BMP-mediated signals from epidermal ectoderm. Cell *82*, 969–979.

Liu, T., Zhang, S., Chen, X., Li, G., and Wang, Y. (2010). Hepatic differentiation of mouse embryonic stem cells in three-dimensional polymer scaffolds. Tissue Eng. Part A *16*, 1115–1122.

Martín, M., Gallego-Llamas, J., Ribes, V., Kedinger, M., Niederreither, K., Chambon, P., Dollé, P., and Gradwohl, G. (2005). Dorsal pancreas agenesis in retinoic acid-deficient Raldh2 mutant mice. Dev. Biol. *284*, 399–411.

Nakano, T., Ando, S., Takata, N., Kawada, M., Muguruma, K., Sekiguchi, K., Saito, K., Yonemura, S., Eiraku, M., and Sasai, Y. (2012). Self-formation of optic cups and storable stratified neural retina from human ESCs. Cell Stem Cell *10*, 771–785.

Niederreither, K., Subbarayan, V., Dollé, P., and Chambon, P. (1999). Embryonic retinoic acid synthesis is essential for early mouse post-implantation development. Nat. Genet. *21*, 444–448.

Nishi, Y., Ji, H., Wong, W.H., McMahon, A.P., and Vokes, S.A. (2009). Modeling the spatio-temporal network that drives patterning in the vertebrate central nervous system. Biochim. Biophys. Acta *1789*, 299–305.

O'Brien, L.E., Jou, T.S., Pollack, A.L., Zhang, Q., Hansen, S.H., Yurchenco, P., and Mostov, K.E. (2001). Rac1 orientates epithelial apical polarity through effects on basolateral laminin assembly. Nat. Cell Biol. *3*, 831–838.

Okada, Y., Shimazaki, T., Sobue, G., and Okano, H. (2004). Retinoic-acid-concentration-dependent acquisition of neural cell identity during in vitro differentiation of mouse embryonic stem cells. Dev. Biol. *275*, 124–142.

Okada, Y., Matsumoto, A., Shimazaki, T., Enoki, R., Koizumi, A., Ishii, S., Itoyama, Y., Sobue, G., and Okano, H. (2008). Spatiotemporal recapitulation of central nervous system development by murine embryonic stem cell-derived neural stem/progenitor cells. Stem Cells *26*, 3086–3098.

Peterson, K.A., Nishi, Y., Ma, W., Vedenko, A., Shokri, L., Zhang, X., McFarlane, M., Baizabal, J.M., Junker, J.P., van Oudenaarden, A., et al. (2012). Neural-specific Sox2 input and differential Gli-binding affinity provide context and positional information in Shh-directed neural patterning. Genes Dev. *26*, 2802–2816.

Placzek, M., Jessell, T.M., and Dodd, J. (1993). Induction of floor plate differentiation by contact-dependent, homeogenetic signals. Development *117*, 205–218.

Pollard, S.M., Benchoua, A., and Lowell, S. (2006). Neural stem cells, neurons, and glia. Methods Enzymol. *418*, 151–169.

Ribes, V., Le Roux, I., Rhinn, M., Schuhbaur, B., and Dollé, P. (2009). Early mouse caudal development relies on crosstalk between retinoic acid, Shh and Fgf signalling pathways. Development *136*, 665–676.

Roelink, H., Porter, J.A., Chiang, C., Tanabe, Y., Chang, D.T., Beachy, P.A., and Jessell, T.M. (1995). Floor plate and motor neuron induction by different concentrations of the amino-terminal cleavage product of sonic hedgehog autoproteolysis. Cell *81*, 445–455.

Sasai, Y., and De Robertis, E.M. (1997). Ectodermal patterning in vertebrate embryos. Dev. Biol. *182*, 5–20.

Sato, T., Vries, R.G., Snippert, H.J., van de Wetering, M., Barker, N., Stange, D.E., van Es, J.H., Abo, A., Kujala, P., Peters, P.J., and Clevers, H. (2009). Single Lgr5 stem cells build crypt-villus structures in vitro without a mesenchymal niche. Nature *459*, 262–265.

Schnapp, E., Kragl, M., Rubin, L., and Tanaka, E.M. (2005). Hedgehog signaling controls dorsoventral patterning, blastema cell proliferation and cartilage induction during axolotl tail regeneration. Development *132*, 3243–3253.

Spence, J.R., Mayhew, C.N., Rankin, S.A., Kuhar, M.F., Vallance, J.E., Tolle, K., Hoskins, E.E., Kalinichenko, V.V., Wells, S.I., Zorn, A.M., et al. (2011). Directed differentiation of human pluripotent stem cells into intestinal tissue in vitro. Nature *470*, 105–109.

Suga, H., Kadoshima, T., Minaguchi, M., Ohgushi, M., Soen, M., Nakano, T., Takata, N., Wataya, T., Muguruma, K., Miyoshi, H., et al. (2011). Self-formation of functional adenohypophysis in three-dimensional culture. Nature *480*, 57–62.

Tickle, C. (1991). Retinoic acid and chick limb bud development. Dev. Suppl. *1*, 113–121.

Vezina, C.M., Allgeier, S.H., Fritz, W.A., Moore, R.W., Strerath, M., Bushman, W., and Peterson, R.E. (2008). Retinoic acid induces prostatic bud formation. Dev. Dyn. *237*, 1321–1333.

Wagner, M., Thaller, C., Jessell, T., and Eichele, G. (1990). Polarizing activity and retinoid synthesis in the floor plate of the neural tube. Nature *345*, 819–822.

Wichterle, H., Lieberam, I., Porter, J.A., and Jessell, T.M. (2002). Directed differentiation of embryonic stem cells into motor neurons. Cell *110*, 385–397.

Yu, W., Datta, A., Leroy, P., O'Brien, L.E., Mak, G., Jou, T.S., Matlin, K.S., Mostov, K.E., and Zegers, M.M. (2005). Beta1-integrin orients epithelial polarity via Rac1 and laminin. Mol. Biol. Cell *16*, 433–445.

Zhu, Y., Carido, M., Meinhardt, A., Kurth, T., Karl, M.O., Ader, M., and Tanaka, E.M. (2013). Three-dimensional neuroepithelial culture from human embryonic stem cells and its use for quantitative conversion to retinal pigment epithelium. PLoS ONE *8*, e54552.